IOP Conf. Series: Materials Science and Engineering **232** (2017) 012025 doi:10.1088/1757-899X/232/1/012025

Comparative study of bearing loads for different twin screw compressor rotor configurations

D Buckney and C Anderson

Howden Compressors, Glasgow, UK

david.buckney@howden.com

Abstract. Designing rotor geometry is a critical stage in the design of a twin screw compressor which has a significant impact on: capacity; leakage characteristics; thermodynamics; rotor stiffness; dynamics; and loading on the bearings. The focus of this paper is on bearing loads. In order to design screw compressors that can operate at higher pressures the bearings quickly become a limiting factor. With the need to house the bearings adjacent to one another on each of the parallel rotor shafts at a given centre distance there is an inherent limit to the bearing geometry envelope. In this investigation the 'rotor configuration' refers to the rotor lobe combination, length to diameter ratio (L/D), and wrap angle. The geometry of the transverse rotor profiles is kept constant, as far as possible, allowing conclusions to be drawn based on a manageable number of variables. A procedure to calculate bearing specific loads based on results from a thermodynamic chamber model is presented and results for a range of rotor configurations are discussed.

1. Introduction

Efficient procedures for calculation of twin screw compressor rotor forces due to pressure loading are well documented [1, 2]. With the availability of FEA / CFD software packages, numerical approaches to force calculation are also commonplace [3, 4]. The current work is based on a numerical procedure that builds on previous work by the authors [5] that allows the pressure curve from a chamber model to be mapped onto the 3D rotor surfaces. Additional calculation steps to calculate bearing forces are presented here.

This investigation is part of wider ranging design work that compared rotor geometry envelopes, weights, lateral stiffness, torsional stiffness, leakage areas, port areas, thermodynamic performance and forces for various rotor configurations. In this paper selected results are presented in order to demonstrate important considerations for high gas load applications.

In order to allow clear presentation of results a nominal reference rotor configuration will be used with a 4/6 lobe combination, 1.375 L/D, and 300° wrap angle. Each of these three variables will be modified one at a time.

2. Rotor design

2.1. Profile generation

Different profile co-ordinates were generated for each lobe combination. Whilst it is easy to linearly scale any existing profile, changing the number of lobes on each profile can potentially cause

unwanted changes to the nature of the profile. Some of the profile parameters that were carefully controlled in this investigation are detailed in Figure 1.

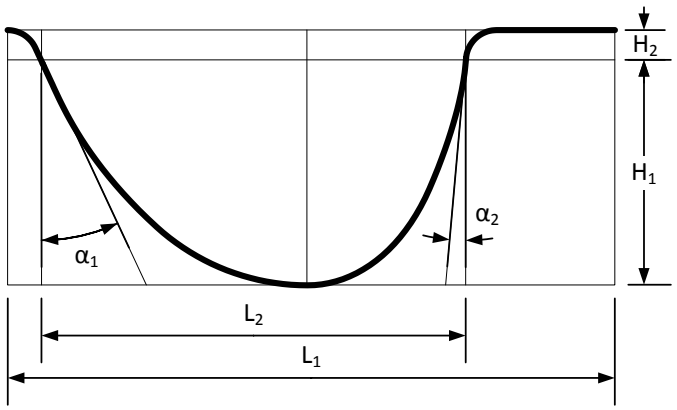

Figure 1. Fixed rotor profile parameters

The parameters α_1 and α_2, which describe the flank angles at the pitch circles, have been kept constant. In order to preserve the relative width of the male and female rotors the ratio L_2/L_1 has been kept constant. This ratio is achieved by adjusting the parameter H_1. When changing the lobe combination, the appearance of the rotors changes a fair amount and preserving the relative width of the lobes at the pitch circles provides a tangible measure that the profile is as similar as possible.

From an optimisation point of view, minimising the parameter H_2 can essentially eliminate the blow hole leakage path. In addition to increasing flow, this parameter is generally non-zero for practical purposes: to maintain a good 'contact' band either side of the pitch radius; and for manufacturability. Therefore it seemed appropriate to keep the ratio H_2/r_{2o} constant, where r_{2o} is the outer radius on the female rotor.

2.2. Rotor normalisation

For each rotor lobe combination the generated profile was used to create rotor bodies for the various combinations of wrap angle and L/D ratio. Rotor models were created using 'SCORG' software [6] in order to calculate rotor characteristics including the volume displacement per revolution of the male rotor, V_c. Each rotor pair was then scaled, or normalised, in order to target V_c equal to 10 litres/rev.

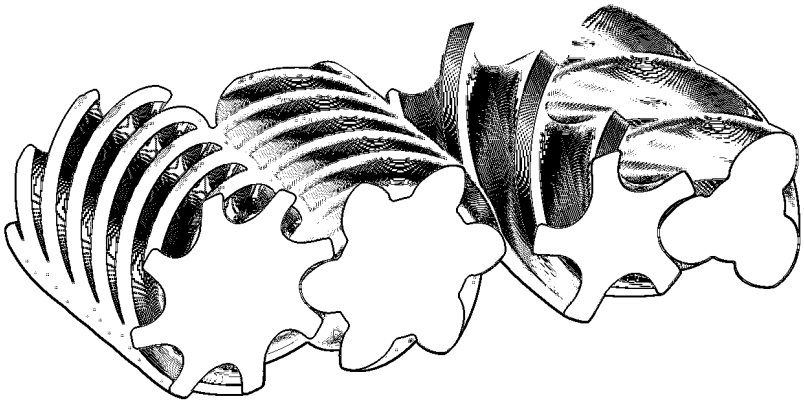

Figure 2. Normalised rotors shown to scale

Examples of two rotor pairs with different lobe combination, wrap angle, and L/D are shown in Figure 2. The 6/8 combination on the left has small compression chambers but more of them resulting in the

same displacement per revolution of the male rotor. The normalised rotor tip diameters (OD) and rotor root diameters (ID) for a selected range of rotor configurations are presented in the results section.

3. Simulation

For each rotor configuration model generated in SCORG, the thermodynamic performance was simulated using a chamber model included in the software package. This model was developed by Stosic et al. [6]. The chosen duty used in this investigation is for oil free compression of methane gas which is representative of common hydrocarbon compression applications. The operating pressures investigated at this stage in the design are actually fairly moderate but are nonetheless adequate to allow relative comparisons between different rotor configurations in terms of thermodynamic performance and pressure loading in this investigation. In the wider study it is planned to repeat comparisons at more specific duties to confirm the current findings and explore the operating limits in more detail. At this stage the simulated power is based only on indicated power of compression and no attempt has been made to model bearing or other parasitic power losses. The adiabatic efficiencies presented in this study are consequently high. The thermodynamic model input parameters are summarised in Table 1.

Table 1. Thermodynamic model parameters

Parameter	Value
Interlobe clearance (mm)	0.15
Radial clearance (mm)	0.15
Axial clearance (mm)	0.1
Volume index, Vi	2.6
Speed, N (rpm)	6000
Suction pressure, p_1 (Bara)	2
Discharge pressure, p_2 (Bara)	7
Suction temperature, T_1 (°C)	40
Ratio of specific heats, γ	1.3
Gas constant, R (J/(kgK))	518.3
Compressibility factor, Z	1

4. Pressure forces

4.1. Pressure distribution

The pressure curve of the instantaneous internal pressure against the male rotor angle is calculated by the chamber model. This pressure distribution can be mapped onto the 3D surface of the rotors using a procedure detailed in previous publications [5]. This local pressure can be described as a function of: the spatial co-ordinates X, Y and Z; and a reference cycle angle, θ, which describes the male rotor position. The resulting pressure distribution on the rotor surfaces, in Pascals, is shown in Figure 3.

4.2. Pressure area and force calculation

The numerical procedure used to calculate the resulting loads utilised discrete force vectors at nodal positions. The location of the node is known along with the pressure at the node therefore the effective pressure area is required in order to calculate the point force.

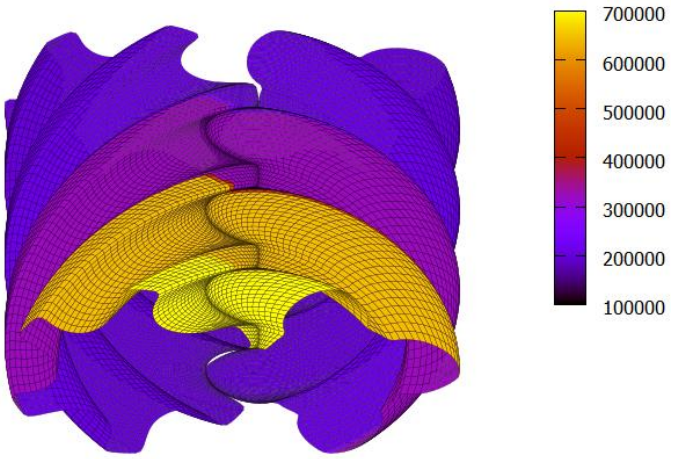

Figure 3. Pressure distribution on rotor surfaces

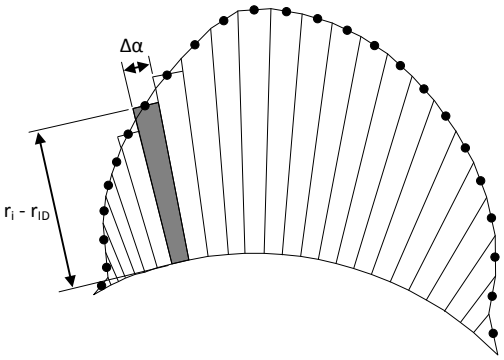

Figure 4. End face pressures

The nodes are equidistant around the transverse rotor profile so length of the profile curve and the number of lobes gives dimension Δs. The nodes are also equidistant along the length so similarly the dimension ΔL is easily calculated. The effective area is calculated in equation (1) where the length must be corrected using the angle, φ_S, which is measured between the surface normal and the transverse plane; this describes the slope when travelling axially along the rotor surface. This angle is affected by both local helix angle and local flank angle on the rotor surface. The force normal to the rotor surface, F_N, is simply calculated using the local pressure and the area as in equation (2).

$$A = \Delta s \frac{\Delta L}{\cos(\varphi_S)} \tag{1}$$

$$F_N = pA \tag{2}$$

The end face pressure forces were approximated using the pressure results and nodes on the end planes of Figure 3. The pressure area over which it was assumed the pressure at each node acts on the end face is shown in Figure 4. The effective rotor body pressure area has been truncated at the root of the rotor for the purposes of this investigation. This assumes that pressure faces on the end faces of the protruding shafts is similar at each end of the rotors and can be neglected. These geometry assumptions can later be readily adapted with preliminary or known rotor shaft details. The total pressure force calculated for each end face is taken as the sum of the individual forces calculated from each local pressure and area:

$$F_{END\ FACE} = \sum_{i=1}^{n} \frac{\Delta\alpha_i}{2}\left(r_i^2 - r_{ID}^2\right)p_i \tag{3}$$

4.3. Calculation of force components

A given point on the rotor surface, at a given rotor position, for which the polar co-ordinate angle, β, and the surface normal angle, φ_{PA}, can be readily calculated is shown in Figure 5. Using these angles, the local transverse flank angle, φ_F, can be found using equation (4).

The force component F_C describes the transverse force tangent to the 'circle' of rotation and F_R is the transverse, radial force. The local helix angle, φ_H, is defined on the plane viewed on A-A which is

the plane tangent to the 'cylinder' of rotation. This is calculated using the local radius and the lead length, h, using equation (5).

Applying equations common for gear theory, the transverse force tangent to the circle of rotation can be found using equation (6). Knowing F_C, basic trigonometric relationships can be applied to find F_x, F_y, and F_A.

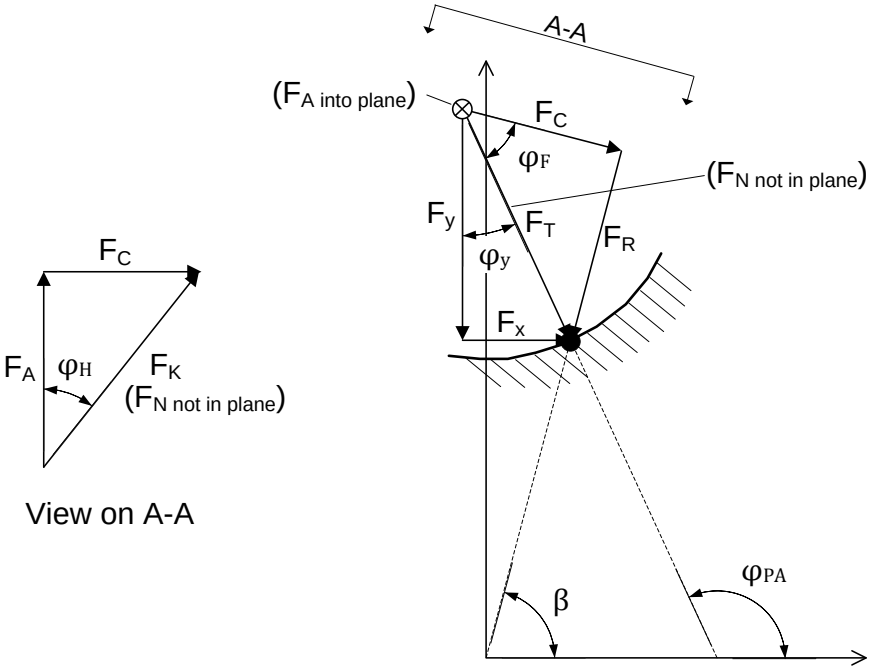

Figure 5. Force vectors on transverse plane

$$\varphi_F = 90 - (\varphi_{PA} - \beta) \tag{4}$$

$$\varphi_H = tan^{-1}\left(\frac{2\pi r}{h}\right) \tag{5}$$

$$F_C = F_N \cos(tan^{-1}(\tan(\varphi_F)\cos(\varphi_H)))\cos(\varphi_H) \tag{6}$$

4.4. Resolving reaction forces

Net forces are readily resolved using static analysis of the rotor bodies once the components F_x, F_y, and F_A, which are aligned to the global Cartesian co-ordinate system, are known. While the rotor torque is only dependent on the geometry of the rotor bodies, the axial and radial forces are somewhat dependent on additional geometry features of the rotor shafts. The assumptions for the end face pressure areas already presented will have a significant effect on the net axial forces. The radial forces are dependent on the axial position of the bearings. In order to evaluate the rotor configurations without assuming shaft dimensions the radial pressure forces were resolved at planes co-incident with the inlet and outlet rotor end faces. This will result in the largest outlet radial forces since moving the bearings away from the rotor body allows the radial load to be shared more evenly between the inlet and outlet end bearings.

5. Results

5.1. Rotor diameters

Normalisation of each rotor pair, whereby the geometry was scaled until the displacement constant was 10 l/rev, resulted in the different rotor sizes as summarized in Figure 6. Generally, increasing the overall number of rotors lobes results in rotors with bigger diameters and unsurprisingly, increasing the relative length (or L/D) results in smaller diameters. Wrap angle has little effect on rotor size. 4/5 and 5/6 lobes combinations result in a considerably smaller female rotor for the same displacement.

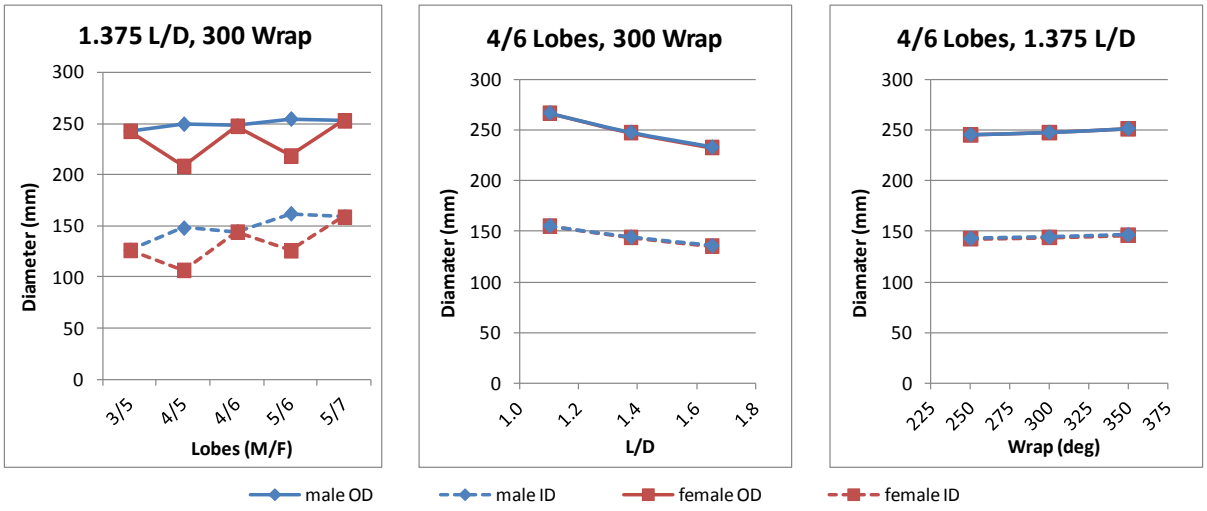

Figure 6. Rotor diameters

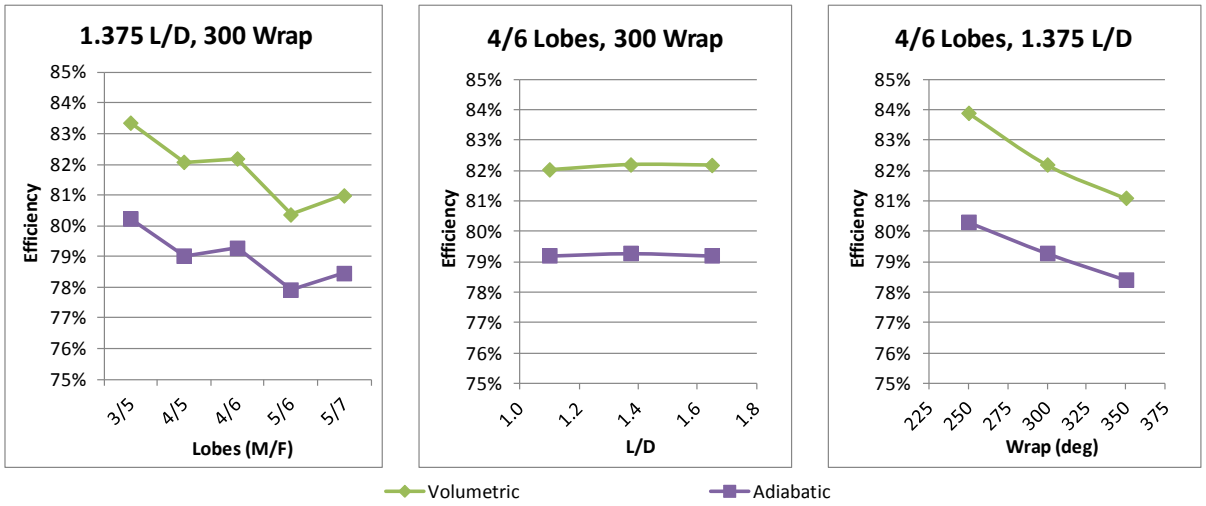

Figure 7. Thermodynamic performance

5.2. Thermodynamic performance

Results from the chamber model are shown in Figure 7. L/D has little effect on thermodynamic performance for the simulated duty. Smaller lobe combinations generally improve efficiency but interestingly 4/6 was slightly better that 4/5 and 5/7 was slightly better than 5/6. Smaller rotor wrap angles shorten the overall cycle time therefore there is less time during which leakage can occur; this is thought to be the reason for the better performance with smaller wrap angles.

5.3. Pressure forces

A summary of the resultant radial forces at the high pressure end is shown in Figure 8. Due to the way the pressure distribution changes as the rotors turn, the resulting forces are not constant therefore the minimum and maximum forces are shown for each rotor. This shows that a smaller number of male rotor lobes or smaller wrap angle results in larger variation in the radial force. In all cases the largest radial force occurs on the female rotor. Between 3/5, 4/6, and 5/7 lobe combinations there is little difference in the maximum radial force whilst in 4/5 and 5/6 this force is smaller. As expected, smaller L/D ratios result in smaller radial forces on both rotors.

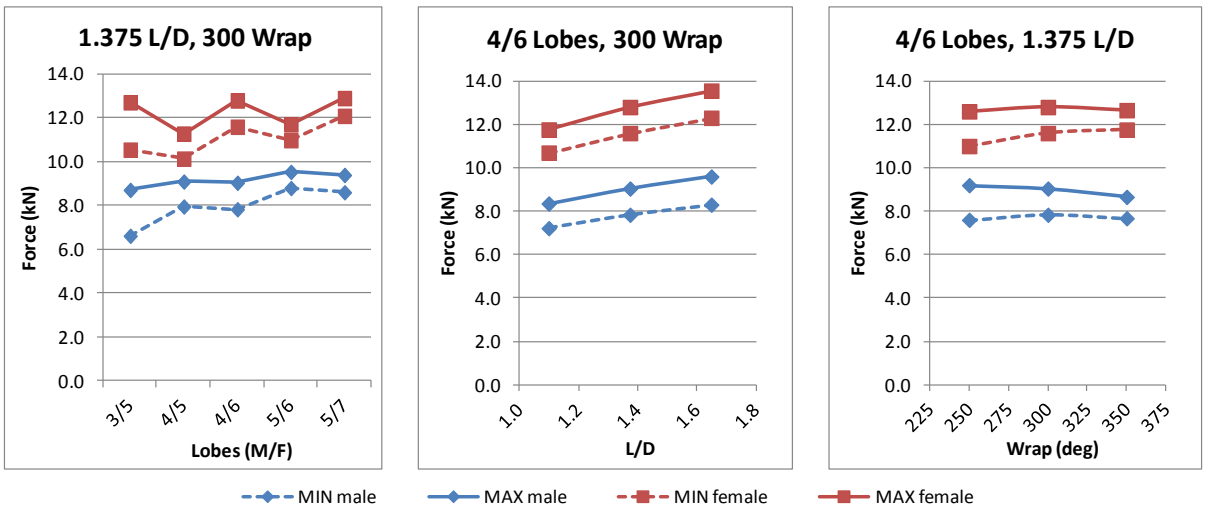

Figure 8. Radial forces at outlet rotor end face

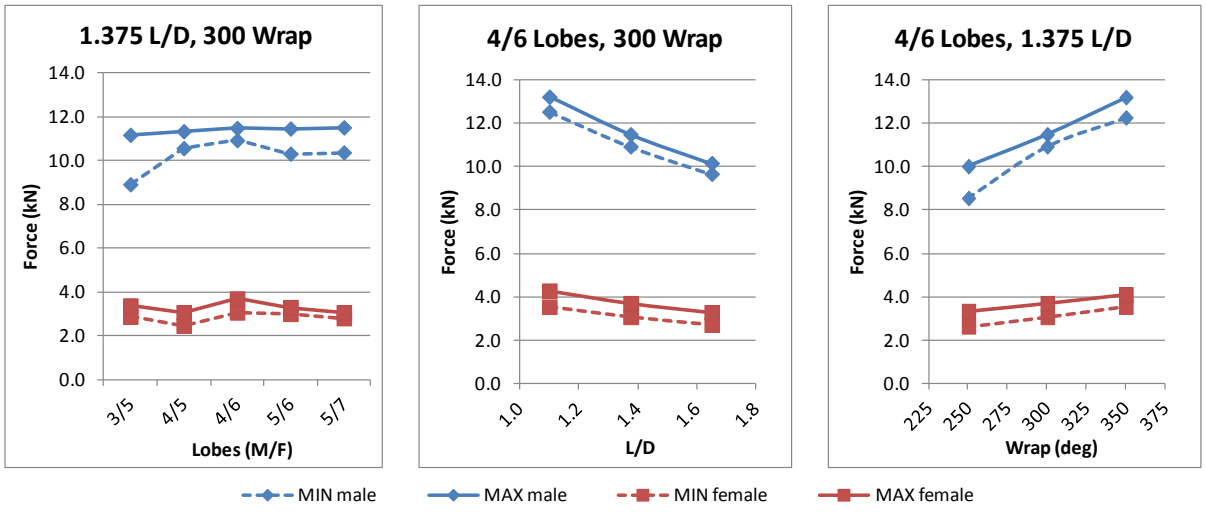

Figure 9. Axial forces

Resultant axial forces are summarised in Figure 9; these are considerably higher for the male rotor than for the female rotor. The lobe combination has little effect on the maximum axial force however the 4/6 lobe combination results in the smallest variation in the axial forces which would provide improved dynamic stability. The reduction in radial forces with reduced L/D (Figure 8) comes at the expense of having larger axial forces (Figure 9). Larger wrap angles increase the axial force; this stands to reason as rotors with zero wrap angle would have zero net axial load.

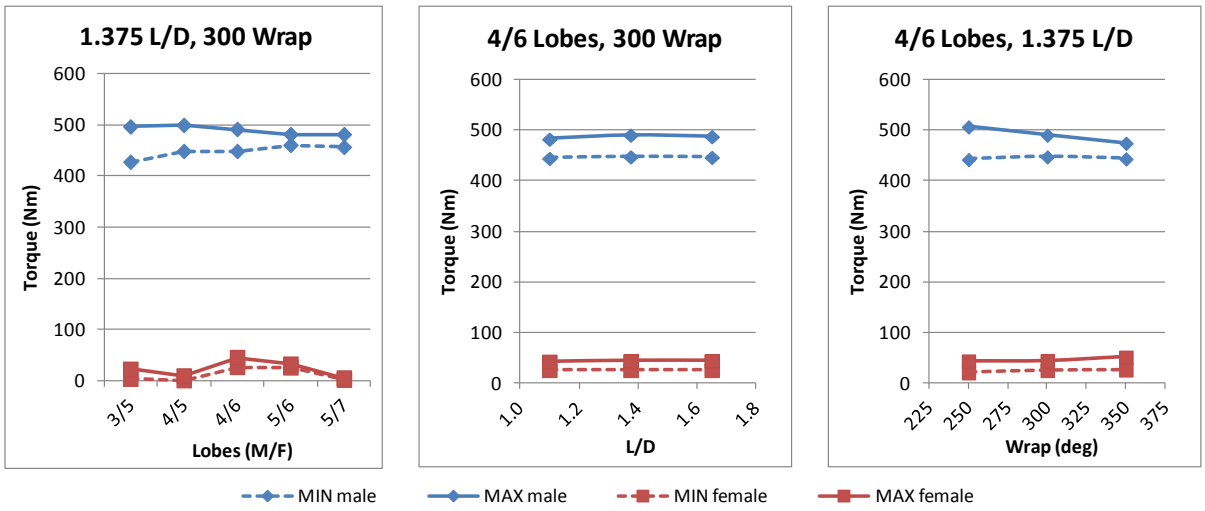

Figure 10. Torque

The rotor torque for each rotor configuration is shown in Figure 10. There isn't a great deal of change in the maximum torque however, as with the radial forces, having more lobes or increasing the wrap angle reduces the variation in the torque. This may be an important factor on high pressure, and consequently high torque, operating duties.

5.4. Bearing specific load

Each rotor configuration introduces inherent limits on the bearing geometry hence the size of bearings that can be accommodated should be considered. Applying some assumptions about the bearing type and geometry will allow some relative comparisons of the bearings for each rotor configuration.

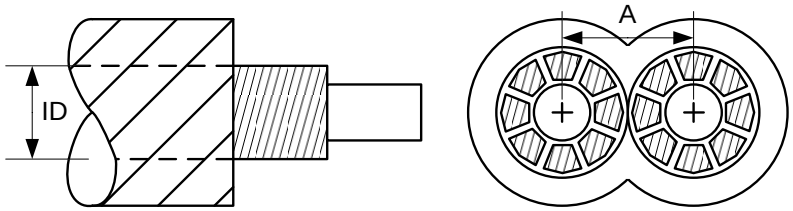

Figure 11. Driving dimensions for bearing area calculation

Hydrodynamic journal bearings are assumed at the outlet radial bearings. The diameter of the journal will be taken as the root diameter, ID, of each respective rotor as shown in Figure 11. In practice, the journal diameter is likely to be a bit smaller for practical reasons. The length of the journal will be taken to be the same as the diameter resulting in an aspect ratio of 1; it is not usually recommended to increase the length of the journal beyond this limit. The male and female root diameters in Figure 6 were simply squared to give the projected area.

The main limitation on the size of the thrust bearings is the outer diameter of the bearing housing, or carrier ring, which, assuming the male and female axial bearings are positioned side by side, will be limited by the rotor centre distance, A. By assuming a typical tilting pad thrust bearing design, the effective thrust surface can be calculated using a factor of 0.42 of the area of the carrier ring, which in this case will have a maximum diameter equal to the centre distance.

These areas for the radial and axial bearings were used, along with the forces in Figure 8 and Figure 9 respectively, to calculate the specific load on the bearings for each rotor configuration. Note that since the radial loads were calculated at the end face of the rotor, and not at the centre of pressure

of the assumed bearing, the load is slightly higher but for the purposes of comparing different rotor configurations this is not significant.

Presenting specific load rather than radial forces in Figure 12 has little change on the trends against L/D and wrap angle however there is a significant change in the results against different lobe combinations: The lower forces in the 4/5 and 5/6 rotors do not offset the reduction in pressure area which is significantly smaller on these female rotors and as a result the specific load is much higher.

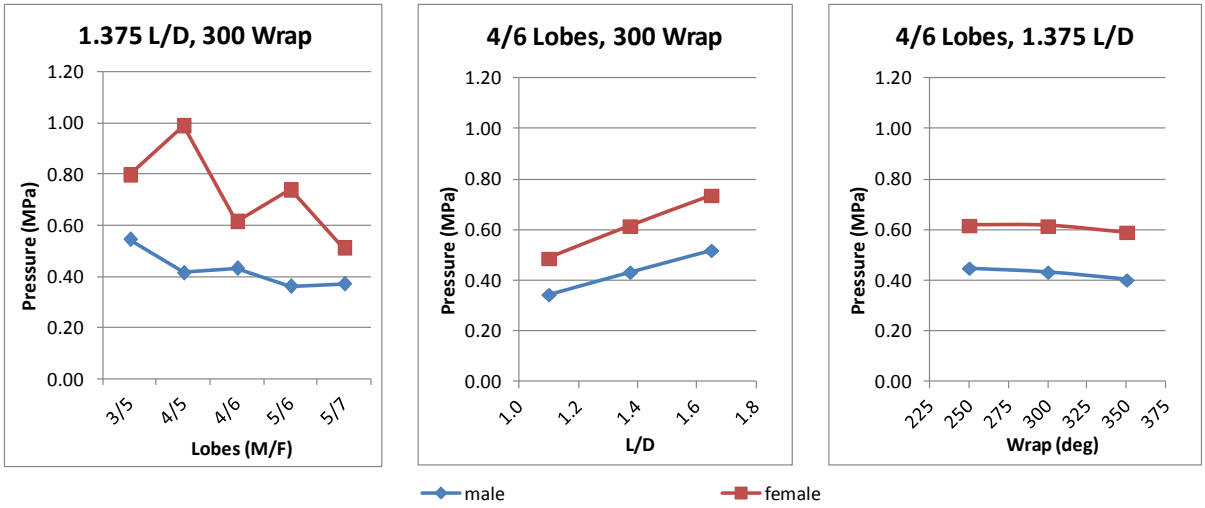

Figure 12. Radial bearing specific loads

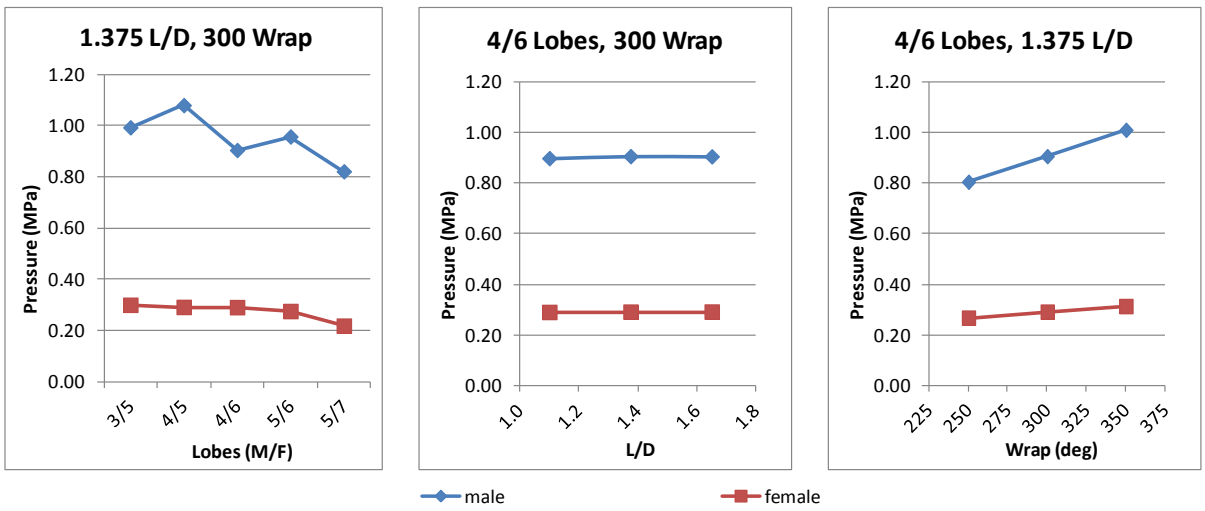

Figure 13. Axial bearing specific loads

Whereas the maximum axial forces were not sensitive to the lobe combination, having more rotor lobes generally reduces the specific load and 4/5 and 5/6 combinations stand out as poor performers as shown in Figure 13. These results suggest that the L/D can safely be reduced, in order to limit the radial bearing pressure, without any increase in the axial bearing pressures since the larger centre distance and bearing size compensate for the higher axial forces predicted in Figure 9. Larger wrap angles increase the specific load on the axial thrust bearings.

6. Conclusions

The female radial bearing at compressor outlet and the male axial thrust bearing are the most critical for design. With the duty investigated in this study, the bearing pressures are all well within realistic operating values. Rather than exploring the actual pressure limitations for a specific rotor configuration this study has provided a general evaluation of the relative performance of different rotor configurations, this is suited for use at an early conceptual design phase.

A key finding is that rotor pairs with only one more female rotor lobe number than male rotor lobe number show both disadvantages in terms of predicted thermodynamic performance and bearing loading which allows these to be ruled out for high pressure design.

Reducing rotor L/D can reduce the radial bearing pressure load without any apparent detriment to the thermodynamic performance and does not result in an increase in the specific load on the thrust bearings. The downside of excessively reducing L/D would be oversized rotor diameters and axial bearings diameters which could result in excessive costs and larger bearing losses as well as higher rotor tip speeds which would ultimately limit the operating speed and capacity.

The results generally seem to suggest smaller rotor wrap angles are better however it may be the case that the current model doesn't adequately capture kinetic losses that would occur due to the higher flow velocities that are a feature of low wrap angle designs. Some refinement of the chamber model setup/ use of CFD would be interesting to shed more light on this.

In general the results predict that having a smaller number of rotor lobes is good in terms of thermodynamic performance but having more lobes is better to reduce bearing loads and load variations. The best lobe combination for a given design will be a trade off based on the specific operating envelope of the designed compressor.

Verification of the bearing forces calculated in this work has so far been limited to comparison to other available software. Work is planned to acquire measured bearing forces from a test compressor.

Further work planned but not available at the time of writing is to include the effect of radial and axial loads introduced by timing gears and also to model the bearing power losses. Appropriately designed gears can be used to mitigate, to some extent, the imbalance between the axial loads on the male and female rotors shown in Figure 13. This imbalance can be further mitigated by decreasing the size of the female thrust bearing in order to accommodate a larger male thrust bearing. The inclusion of power losses will change the adiabatic efficiency results presented in Figure 7 and would be useful to allow quantification of performance penalties.

References

[1] Stosic N, Smith IK and Kovacevic A 2005 *Screw Compressors: Mathematical Modelling and Performance Calculation* London

[2] You CX, Tang Y, Fleming JS, and Tramschek AB 1994 A generalized computer program for calculating the bearing loads in helical twin screw compressors *International Compressor Engineering Conference at Purdue* Paper 1051

[3] Hsu RH, Wu YR, Wu WT, and Tran VT 2015 Rotor load analysis method for twin screw compressors with considering gaseous pressure and working temperature *14th International Federation for the Promotion of Mechanism and Machine Science* Taipei

[4] Wu HG, Ma Y, and Xing ZW 2004 Theoretical and experimental investigation of compressor loads in twin screw compressor *International Compressor Engineering Conference at Purdue* Paper 1701

[5] Buckney D, Kovacevic A, and Stosic N 2016 Design and evaluation of rotor clearances for oil-injected screw compressors *Proc IMechE Part E: J Process and Mechanical Engineering* **231** pp 26-37

[6] Hanjalic K and Stosic N 1997 Development and optimization of screw machines with a simulation model - Part II: thermodynamic performance simulation and design optimization *J Fluids Eng Trans ASME* **119** pp 664-670

[7] SCORG online documentation *http://pdmanalysis.co.uk/online-documentation* 24/05/2017